OPEN ACCESS

University of BRISTOL

Wu, Z., & Cooper, J. (2016). Active Flutter Suppression Combining the Receptance Method and Flutter Margin. In *57th AIAA/ASCE/AHS/ASC Structures, Structural Dynamics, and Materials Conference* [AIAA 2016-1227] American Institute of Aeronautics and Astronautics Inc. (AIAA). https://doi.org/10.2514/6.2016-1227

Peer reviewed version

Link to published version (if available):
10.2514/6.2016-1227

Link to publication record in Explore Bristol Research
PDF-document

University of Bristol - Explore Bristol Research
General rights

This document is made available in accordance with publisher policies. Please cite only the published version using the reference above. Full terms of use are available:
http://www.bristol.ac.uk/red/research-policy/pure/user-guides/ebr-terms/

Active Flutter Suppression Combining the Receptance Method and Flutter Margin

Zhigang Wu*
Beihang University, Beijing, 100191, China

Jonathan E. Cooper†
University of Bristol, Bristol, BS8 1TR, UK

Active flutter suppression is used to prevent flutter throughout the flight envelope by supplying active control forces in response to vehicle motions. In recent years, studies have been conducted on active flutter suppression using the receptance method. The advantage of the receptance method is that the feedback control gains are purely based upon measured receptances, without any need to evaluate or know the mass, damping, and stiffness matrices of the system. However, determination of the desired closed-loop poles is a unsolved problem. The goal of this work is to determine the pole-assignment in the receptance method, enabling the extension of flutter boundaries by combining the receptance method with the flutter margin technique. The design of an output feedback control for a multi-degree-of-freedom uniform wing numerical model with a trailing-edge control surface is demonstrated. Numerical results show that the presented approach can effectively extend the flutter boundary without the usual difficulties of pole-assignment.

I. Introduction

Active flutter suppression (AFS) has the goal of preventing flutter, an instability phenomenon resulting from the coupling between the structure and aerodynamic forces which can lead to catastrophic structural failure.[1] Through the combination of aeroelasticity and active controls (aeroservoelasticity), the active aeroelastic technique (AAT) has had much research focus over the past several decades, and is likely to play an important role in the design of contemporary and next-generation advanced air vehicles. Instead of passive modification of structural mass or stiffness, AAT can improve the aeroelastic characteristics and flight performance by supplying active control forces responding to inputs from sensors around the aircraft.

Over the past several decades, a large number of control strategies had been developed for active flutter suppression using classical and modern control theory, such as PID control,[2] pole-assignment method,[3] LQR and LQG control,[4] H_∞ control, μ-synthesis,[5] neural-network control,[6] etc.

In recent years, the receptance method has been developed for active vibration control by Mottershead et al.[7,8] The advantage of this method is that the feedback control gains are purely based upon measured receptances, without any need to evaluate or know the mass, damping, and stiffness matrices of the system. The suppression of flutter may be considered as an inverse eigenvalue problem,[9] and plenty of research has been conducted on active flutter suppression using the receptance method.

Some numerical examples demonstrated the control gains obtained by the receptance method can effectively extend the flutter envelope by adjusting poles of the system.[10,11] Papatheou et al. demonstrated an experimental study involving the implementation of the method of receptances to control binary flutter in a wind-tunnel aerofoil rig.[12] Singh developed a multiple-input state and output feedback control strategy associated with wings having multiple control surfaces based upon the receptance method.[13] Tehrani et al. have extended the receptance method to a class of single-degree-of-freedom nonlinear systems characterised using describing functions to achieve active vibration control with state feedback.[14] Zhen et al. presented a modified receptance method for obtaining the time-varying receptances of a general nonlinear system, and then applied the method to to a structurally nonlinear aeroelastic system for active flutter suppression.[15]

*Associate professor, School of Aeronautic Science and Engineering, wuzhigang@buaa.edu.cn, member of AIAA
†RAEng Airbus Sir George White Professor of Aerospace Engineering, Department of Aerospace Engineering, j.e.cooper@bristol.ac.uk, Associate Fellow of AIAA

By using the receptance method, the feedback control gains can be obtained based upon the receptances of the open-loop poles and desired closed-loop poles. However, there is a common unsolved problem in above research, that is how to determine appropriate values of the desired poles. In fact, inappropriate pole-assignment can result in false or inconsistent control gains, which may deteriorate the flutter boundary, possibly due to exceeding control surface rate or deflection limits.

The objective of this work is to overcome the difficulties of pole-assignment in the receptance method for extension of flutter boundary by using the combination of the receptance method and flutter margin. Following mathematical treatment of the problem, the design of an output feedback control for a multi-degree-of-freedom uniform wing with one trailing-edge control surface is demonstrated. Numerical results show that the presented approach can effectively extend the flutter boundary without difficulties of the traditional pole-assignment method.

II. Aeroelastic Modeling

Without loss of generality, a uniform cantilever wing is chosen as the object of study, as shown in Fig. 1. Its span is l, and chord is c. x_f denotes the position of the flexural axis. The bending and torsional stiffness are EI and GJ respectively, and the mass of unit area is m. Two sensors are located on the corners of the wing tip and can measure the vibration of the structure, and a trailing-edge control surface can produce aerodynamic control force.

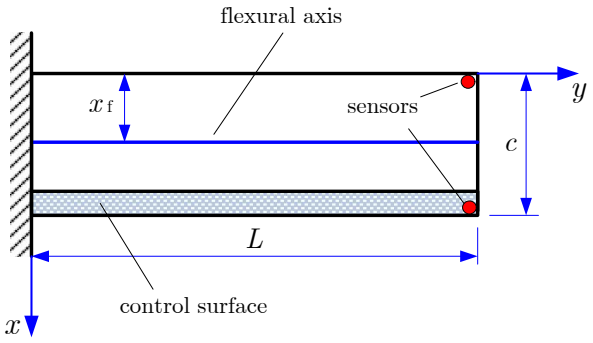

Figure 1. The Platform of the Rectangular Wing

The deformation of the wing $w(x, y, t)$ can be seen as the combination of bending and torsion of the flexural axis, that is

$$w(x, y, t) = h(y, t) + (x - x_\mathrm{f})\theta(y, t) \tag{1}$$

where $h(y, t)$ and $\theta(y, t)$ are bending deflection and twist angle of the flexural axis respectively. By using the assumed modal shape method, $h(y, t)$ and $\theta(y, t)$ can be expressed as

$$h(y, t) = \sum_{i=1}^{n_\mathrm{b}} \phi_{\mathrm{B}i}(y) q_{\mathrm{B}i}(t), \qquad \phi_{\mathrm{B}i}(y) = \left(\frac{y}{l}\right)^{i+1} \tag{2}$$

$$\theta(y, t) = \sum_{j=1}^{n_\mathrm{t}} \phi_{\mathrm{T}j}(y) q_{\mathrm{T}j}(t), \qquad \phi_{\mathrm{T}j}(y) = \left(\frac{y}{l}\right)^{j} \tag{3}$$

where $q_{\mathrm{B}i}(t)$ and $q_{\mathrm{T}j}(t)$ are the generalized coordinates, $\phi_{\mathrm{B}i}(y)$ and $\phi_{\mathrm{T}j}(y)$ are the assumed modal shape functions, n_b and n_t are the numbers of bending modes and torsional modes respectively.

Applying Eq. (1)–(3), the kinetic energy of the wing can be obtained as

$$\begin{aligned} T &= \frac{1}{2}\int_0^l \int_0^c m\dot{w}^2 \,\mathrm{d}x\mathrm{d}y = \frac{1}{2}m\int_0^l \int_0^c \left[\dot{h} + (x - x_\mathrm{f})\dot{\theta}\right]^2 \mathrm{d}x\mathrm{d}y \\ &= \frac{1}{2}m\int_0^l \int_0^c \left[\sum_{i=1}^{n_\mathrm{b}} \phi_{\mathrm{B}i}\dot{q}_{\mathrm{B}i} + (x - x_\mathrm{f})\sum_{j=1}^{n_\mathrm{t}} \phi_{\mathrm{T}j}\dot{q}_{\mathrm{T}j}\right]^2 \mathrm{d}x\mathrm{d}y \end{aligned} \tag{4}$$

and the elastic potential energy is also obtained as

$$\begin{aligned} U &= \frac{1}{2}\int_0^l EI\left(\frac{\partial^2 h}{\partial y^2}\right)^2 \mathrm{d}y + \frac{1}{2}\int_0^l GJ\left(\frac{\partial \theta}{\partial y}\right)^2 \mathrm{d}y \\ &= \frac{1}{2}EI\int_0^l \left(\sum_{i=1}^{n_\mathrm{b}} \frac{\mathrm{d}^2\phi_{\mathrm{B}i}}{\mathrm{d}y^2} q_{\mathrm{B}i}\right)^2 \mathrm{d}y + \frac{1}{2}GJ\int_0^l \left(\sum_{j=1}^{n_\mathrm{t}} \frac{\mathrm{d}\phi_{\mathrm{T}j}}{\mathrm{d}y} q_{\mathrm{T}j}\right)^2 \mathrm{d}y \end{aligned} \tag{5}$$

To evaluate the aerodynamic forces, quasi-steady strip theory is adopted which is a viable approach for low speed, high aspect ratio unswept wings. Note that the aeroelastic models used here are purely to demonstrate the effectiveness of the approach on a representative system. For each strip with span $\mathrm{d}y$, the aerodynamic lift and moment are calculated by

$$\mathrm{d}L = \frac{1}{2}\rho V^2 c C_l^\theta \left(\frac{\dot{h}}{V} + \theta\right)\mathrm{d}y + \frac{1}{2}\rho V^2 c C_l^\beta \beta\, \mathrm{d}y \tag{6}$$

$$\mathrm{d}M = \frac{1}{2}\rho V^2 c C_l^\theta (x_\mathrm{f} - \frac{1}{4}c)\left(\frac{\dot{h}}{V} + \theta\right)\mathrm{d}y + \frac{1}{2}\rho V^2 c^2 C_m^{\dot\theta}\left(\frac{\dot\theta c}{4V}\right)\mathrm{d}y + \frac{1}{2}\rho V^2 c^2 C_m^\beta \beta\, \mathrm{d}y \tag{7}$$

where ρ is density of air, V is airspeed, β is the deflection of control surface, $C_l^\theta, C_l^\beta, C_m^{\dot\theta}, C_m^\beta$ are aerodynamic derivatives and control derivatives. Note that the virtual work of resulting from the aerodynamic forces is

$$\begin{aligned} \delta W &= -\int_0^l \delta h\, \mathrm{d}L + \int_0^l \delta\theta\, \mathrm{d}M \\ &= -\int_0^l \left(\sum_{i=1}^{n_\mathrm{b}} \phi_{\mathrm{B}i}\delta q_{\mathrm{B}i}\right)\mathrm{d}L + \int_0^l \left(\sum_{j=1}^{n_\mathrm{t}} \phi_{\mathrm{T}j}\delta q_{\mathrm{T}j}\right)\mathrm{d}M \end{aligned} \tag{8}$$

and then the generalized aerodynamic forces can be derived as

$$\begin{aligned} Q_{\mathrm{B}k} &= \frac{\partial(\delta W)}{\partial(\delta q_{\mathrm{B}k})} = -\int_0^l \phi_{\mathrm{B}k}\, \mathrm{d}L \\ &= -\frac{1}{2}\rho V^2 c C_l^\theta \int_0^l \phi_{\mathrm{B}k}\left(\frac{1}{V}\sum_{i=1}^{n_\mathrm{b}} \phi_{\mathrm{B}i}\dot{q}_{\mathrm{B}i} + \sum_{j=1}^{n_\mathrm{t}} \phi_{\mathrm{T}j} q_{\mathrm{T}j}\right)\mathrm{d}y - \frac{1}{2}\rho V^2 c C_l^\beta \beta \int_0^l \phi_{\mathrm{B}k}\, \mathrm{d}y \end{aligned} \tag{9}$$

$$\begin{aligned} Q_{\mathrm{T}k} &= \frac{\partial(\delta W)}{\partial(\delta q_{\mathrm{T}k})} = \int_0^l \phi_{\mathrm{T}k}\, \mathrm{d}M \\ &= \frac{1}{2}\rho V^2 c C_l^\theta (x_\mathrm{f} - \frac{1}{4}c)\int_0^l \phi_{\mathrm{T}k}\left(\frac{1}{V}\sum_{i=1}^{n_\mathrm{b}} \phi_{\mathrm{B}i}\dot{q}_{\mathrm{B}i} + \sum_{j=1}^{n_\mathrm{t}} \phi_{\mathrm{T}j} q_{\mathrm{T}j}\right)\mathrm{d}y \\ &\quad + \frac{1}{2}\rho V^2 c^2 C_m^{\dot\theta}\int_0^l \phi_{\mathrm{T}k}\left(\frac{c}{4V}\sum_{j=1}^{n_\mathrm{t}} \phi_{\mathrm{T}j}\dot{q}_{\mathrm{T}j}\right)\mathrm{d}y + \frac{1}{2}\rho V^2 c^2 C_m^\beta \beta \int_0^l \phi_{\mathrm{T}k}\, \mathrm{d}y \end{aligned} \tag{10}$$

Substituting the kinetic energy Eq. (4), the elastic potential energy Eq. (5), and the generalized aerodynamic forces Eq. (9)(10) into the Lagrangian equation

$$\frac{\mathrm{d}}{\mathrm{d}t}\left(\frac{\partial T}{\partial \dot{q}_i}\right) - \frac{\partial T}{\partial q_i} + \frac{\partial U}{\partial q_i} = Q_i \tag{11}$$

and then the equation of motion of the wing is obtained as

$$\begin{bmatrix} \mathbf{A}_{\mathrm{BB}} & \mathbf{A}_{\mathrm{BT}} \\ \mathbf{A}_{\mathrm{TB}} & \mathbf{A}_{\mathrm{TT}} \end{bmatrix}\begin{bmatrix} \ddot{\mathbf{q}}_\mathrm{B} \\ \ddot{\mathbf{q}}_\mathrm{T} \end{bmatrix} + \rho V \begin{bmatrix} \mathbf{B}_{\mathrm{BB}} & \mathbf{B}_{\mathrm{BT}} \\ \mathbf{B}_{\mathrm{TB}} & \mathbf{B}_{\mathrm{TT}} \end{bmatrix}\begin{bmatrix} \dot{\mathbf{q}}_\mathrm{B} \\ \dot{\mathbf{q}}_\mathrm{T} \end{bmatrix} + \left(\rho V^2 \begin{bmatrix} \mathbf{C}_{\mathrm{BB}} & \mathbf{C}_{\mathrm{BT}} \\ \mathbf{C}_{\mathrm{TB}} & \mathbf{C}_{\mathrm{TT}} \end{bmatrix} + \begin{bmatrix} \mathbf{E}_{\mathrm{BB}} & \mathbf{0} \\ \mathbf{0} & \mathbf{E}_{\mathrm{TT}} \end{bmatrix}\right)\begin{bmatrix} \mathbf{q}_\mathrm{B} \\ \mathbf{q}_\mathrm{T} \end{bmatrix} = \rho V^2 \begin{bmatrix} \mathbf{b}_\mathrm{B} \\ \mathbf{b}_\mathrm{T} \end{bmatrix}\beta \tag{12}$$

where $\mathbf{q}_\mathrm{B} = [q_{\mathrm{B}1} \cdots q_{\mathrm{B}n_\mathrm{b}}]^\mathrm{T}$ and $\mathbf{q}_\mathrm{T} = [q_{\mathrm{T}1} \cdots q_{\mathrm{T}n_\mathrm{t}}]^\mathrm{T}$ are the generalized coordinate vectors, $\mathbf{A}$ is the generalized mass matrix, $\mathbf{E}$ is the generalized stiffness matrix, $\mathbf{B}$, $\mathbf{C}$, and $\mathbf{b}$ are the aerodynamic influence coefficient matrices, subscript B and T denote bending modes and torsional modes respectively.

Considering the sensors located in the corners of the wing-tip, the vertical displacements of the receiver points can be expressed as

$$\begin{bmatrix} w_1 \\ w_2 \end{bmatrix} = \begin{bmatrix} \phi_{\mathrm{B}1}(l) & \cdots & \phi_{\mathrm{B}n_\mathrm{b}}(l) & -x_\mathrm{f}\phi_{\mathrm{T}1}(l) & \cdots & -x_\mathrm{f}\phi_{\mathrm{T}n_\mathrm{t}}(l) \\ \phi_{\mathrm{B}1}(l) & \cdots & \phi_{\mathrm{B}n_\mathrm{b}}(l) & (c-x_\mathrm{f})\phi_{\mathrm{T}1}(l) & \cdots & (c-x_\mathrm{f})\phi_{\mathrm{T}n_\mathrm{t}}(l) \end{bmatrix} \begin{bmatrix} \mathbf{q}_\mathrm{B} \\ \mathbf{q}_\mathrm{T} \end{bmatrix} \tag{13}$$

Eq. (12) and (13) are the equations of motion of the open-loop aeroelastic system, and can be denoted simply as

$$\mathbf{A}\ddot{\mathbf{q}} + \rho V \mathbf{B}\dot{\mathbf{q}} + (\rho V^2 \mathbf{C} + \mathbf{E})\mathbf{q} = \rho V^2 \mathbf{b}\beta \tag{14}$$

$$\mathbf{w} = \mathbf{D}\mathbf{q} \tag{15}$$

where $\mathbf{A}$, $\mathbf{B}$, $\mathbf{C}$, $\mathbf{D}$, $\mathbf{E}$ and $\mathbf{b}$ are matrices with constant elements, which can be obtained from the properties of mass, stiffness, and aerodynamics of the system. It should be noted that these system matrices are not required for the active flutter suppression by using the receptance method, they are derived for numerical simulation purposes and the virtual testing to validate the methodology.

III. Active Flutter Suppression

A. The Receptance Method

Considering the control surface deflection command as input, and displacement vector $\mathbf{w}$ as output, the receptance matrix (transfer functions) of the open-loop can be obtained based on Eq. (14) and (15)

$$\mathbf{h}(s) = \rho V^2 \mathbf{D} \left[\mathbf{A}s^2 + \rho V \mathbf{B}s + (\rho V^2 \mathbf{C} + \mathbf{E})\right]^{-1} \mathbf{b}r(s) \tag{16}$$

where $r(s)$ denotes the transfer function of the actuator.

As the output feedback control is discussed in current work, so the control law can be expressed as

$$\beta(s) = \beta_0(s)r(s) - (\mathbf{g} + s\mathbf{f})^\mathrm{T}\mathbf{w}(s)r(s) \tag{17}$$

where β_0 is the referenced input, and $\mathbf{g}$, $\mathbf{f}$ are feedback control gain matrices with the dimension of $m \times 1$. For the aeroelastic model shown in Fig. 1, $m = 2$. Then the receptance matrix of the closed-loop is derived as follow

$$\hat{\mathbf{h}}(s) = \rho V^2 \mathbf{D} \left[\mathbf{A}s^2 + \rho V \mathbf{B}s + (\rho V^2 \mathbf{C} + \mathbf{E}) + \rho V^2 \mathbf{b}(\mathbf{g} + s\mathbf{f})^\mathrm{T}\mathbf{D}\right]^{-1} \mathbf{b}r(s) \tag{18}$$

According to the Sherman-Morrison formula,[16] Eq. (18) can be simplified as

$$\hat{\mathbf{h}}(s) = \mathbf{h}(s) - \frac{\mathbf{h}(s)(\mathbf{g} + s\mathbf{f})^\mathrm{T}\mathbf{h}(s)}{1 + (\mathbf{g} + s\mathbf{f})^\mathrm{T}\mathbf{h}(s)} \tag{19}$$

For the problem of stability, the characteristic polynomial of the closed-loop system is

$$1 + (\mathbf{g} + s\mathbf{f})^\mathrm{T}\mathbf{h}(s) = 0 \tag{20}$$

If the desired values of the poles are given as $\{\mu_1, \mu_2, \ldots, \mu_{2n}\}$, they should satisfy

$$1 + (\mathbf{g} + \mu_i \mathbf{f})^\mathrm{T}\mathbf{h}(\mu_i) = 0, \qquad i = 1, 2, \ldots, 2n \tag{21}$$

Re-arranging and combining Eq. (21) into a single matrix expression leads to

$$\begin{bmatrix} \mathbf{h}^\mathrm{T}(\mu_1) & \mu_1 \mathbf{h}^\mathrm{T}(\mu_1) \\ \mathbf{h}^\mathrm{T}(\mu_2) & \mu_2 \mathbf{h}^\mathrm{T}(\mu_2) \\ \vdots & \vdots \\ \mathbf{h}^\mathrm{T}(\mu_{2n}) & \mu_{2n} \mathbf{h}^\mathrm{T}(\mu_{2n}) \end{bmatrix}_{2n \times 2m} \begin{bmatrix} \mathbf{g} \\ \mathbf{f} \end{bmatrix}_{2m \times 1} = \begin{bmatrix} -1 \\ -1 \\ \vdots \\ -1 \end{bmatrix}_{2n \times 1} \tag{22}$$

so the control gains $\mathbf{g}$ and $\mathbf{f}$ can be determined by solving Eq. (**??**). If $m = n$, that is state feedback control, there is a unique solution for the linear algebraic equations. While $m < n$, a linear least squares solution should be conducted.

It should be noted that the receptance matrix of aeroelastic system $\mathbf{h}(\mu_i)$ is dependent on airspeed V. For a given value of V, the frequency response functions of the open-loop can be measured on discrete frequencies, and the receptance matrix $\mathbf{h}(s)$ can be approximated by rational fraction polynomials.[17] If the desired values of the poles μ_i, $i = 1, 2, \cdots$ at a design point (airspeed is V) are determined, the control gains $\mathbf{g}$ and $\mathbf{f}$ can be obtained using the receptance method.

There are some difficulties in implementation of active control using the receptance method. Firstly, proper pole-assignment is very important for flutter suppression. Without prior knowledge of the system, the desired values of the closed-loop poles are hard to be defined, especially for high-order model. Secondly, it is difficult to evaluate the flutter boundary if pole-assignment is achieved for single design point. Finally, due to the receptance $\mathbf{h}(s)$ depending on the airspeed, the obtained control gains may be inconsistent for multiple design points.

B. Flutter Margin

To evaluate the flutter boundary based on the closed-loop poles at subcritical airspeeds, the flutter margin method[18,19] is applied. For a two-degree-of-freedom aeroelastic system, the flutter margin can be expressed as

$$\begin{aligned} F = &\left[\left(\frac{\omega_2^2 - \omega_1^2}{2}\right) + \left(\frac{\beta_2^2 - \beta_1^2}{2}\right)\right]^2 + 4\beta_2\beta_1\left[\left(\frac{\omega_2^2 + \omega_1^2}{2}\right) + 2\left(\frac{\beta_2 + \beta_1}{2}\right)^2\right] \\ &- \left[\left(\frac{\beta_2 - \beta_1}{\beta_2 + \beta_1}\right)\left(\frac{\omega_2^2 - \omega_1^2}{2}\right) + 2\left(\frac{\beta_2 + \beta_1}{2}\right)^2\right]^2 \end{aligned} \tag{23}$$

where $\beta_1 \pm \mathrm{i}\omega_1$, $\beta_2 \pm \mathrm{i}\omega_2$ are the roots of the flutter characteristic equation. Though Eq. (23) is derived from a binary aeroelastic system, its effectiveness in bending-torsion flutter prediction of many real multi-degree-of-freedom aeroelastic system was also demonstrated. It is then possible, using Eq. (23), to evaluate the flutter margin corresponding to any selected airspeed based on the poles of the flutter modes.

According to Zimmerman's paper,[18] if the lift slope C_l^θ can be considered a constant, the flutter margin F has a particularly convenient relationship with dynamic pressure. Regardless of variations in air density ρ, the relationship can be written as follows

$$F = \lambda_2 V^4 + \lambda_1 V^2 + \lambda_0 \tag{24}$$

where λ_0, λ_1, and λ_2 are configuration constants. Eq. (24) is called the "flutter prediction equation". It is not necessary to know anything about the configuration details for the evaluation of λ_i. Using the available data at some subcritical speeds, the coefficients λ_i can be evaluated and the flutter boundary predicted. To improve the accuracy of flutter prediction, it is suggested that data points are taken at closer intervals to define a more precise curve, or to add data points with increasing airspeed.

C. Combination of Receptance Method and Flutter Margin

Firstly, several airspeed design points $\{V_1, V_2, \cdots, V_k\}$ should be selected, where k denotes number of design points, and then the open-loop receptances $\mathbf{h}_j(s)$, $j = 1, \cdots, k$ at all the design points are obtained from experiments or numerical simulations.

According to the flutter margin method, for the jth design point, denoting F_j as the desired flutter margin, we have

$$F(\beta_{1j}, \omega_{1j}, \beta_{2j}, \omega_{2j}) - F_j = 0 \tag{25}$$

where $\beta_{1j} \pm \mathrm{i}\omega_{1j}$ and $\beta_{2j} \pm \mathrm{i}\omega_{2j}$ are the closed-loop poles of flutter modes at airspeed V_j. According to the receptance method, the four poles should satisfy the equations as

$$1 + \big(\mathbf{g} + (\beta_{1j} \pm \mathrm{i}\omega_{1j})\mathbf{f}\big)^{\mathrm{T}}\mathbf{h}_j(\beta_{1j} \pm \mathrm{i}\omega_{1j}) = 0 \tag{26a}$$

$$1 + \big(\mathbf{g} + (\beta_{2j} \pm \mathrm{i}\omega_{2j})\mathbf{f}\big)^{\mathrm{T}}\mathbf{h}_j(\beta_{2j} \pm \mathrm{i}\omega_{2j}) = 0 \tag{26b}$$

To evaluate F_j in Eq. (25), the desired flutter boundary V_f and two undetermined coefficients k_1 and k_2 are introduced, and the flutter prediction equation Eq. (24) can be rewritten as follow

$$F = k_1(V^2 - V_\mathrm{f}^2) + k_2(V^2 - V_\mathrm{f}^2)^2 \tag{27}$$

For the jth design point, we have

$$F_j = k_1(V_j^2 - V_\mathrm{f}^2) + k_2(V_j^2 - V_\mathrm{f}^2)^2 \tag{28}$$

Combining Eq. (25), (26), and (28) leads to the set of equations

$$F(\beta_{1j}, \omega_{1j}, \beta_{2j}, \omega_{2j}) - k_1(V_j^2 - V_\mathrm{f}^2) - k_2(V_j^2 - V_\mathrm{f}^2)^2 = 0, \qquad j = 1, \cdots, k \tag{29a}$$

$$1 + \left(\mathbf{g} + (\beta_{1j} + \mathrm{i}\omega_{1j})\mathbf{f}\right)^\mathrm{T} \mathbf{h}_j(\beta_{1j} + \mathrm{i}\omega_{1j}) = 0, \qquad j = 1, \cdots, k \tag{29b}$$

$$1 + \left(\mathbf{g} + (\beta_{1j} - \mathrm{i}\omega_{1j})\mathbf{f}\right)^\mathrm{T} \mathbf{h}_j(\beta_{1j} - \mathrm{i}\omega_{1j}) = 0, \qquad j = 1, \cdots, k \tag{29c}$$

$$1 + \left(\mathbf{g} + (\beta_{2j} + \mathrm{i}\omega_{2j})\mathbf{f}\right)^\mathrm{T} \mathbf{h}_j(\beta_{2j} + \mathrm{i}\omega_{2j}) = 0, \qquad j = 1, \cdots, k \tag{29d}$$

$$1 + \left(\mathbf{g} + (\beta_{2j} - \mathrm{i}\omega_{2j})\mathbf{f}\right)^\mathrm{T} \mathbf{h}_j(\beta_{2j} - \mathrm{i}\omega_{2j}) = 0, \qquad j = 1, \cdots, k \tag{29e}$$

The above equations are the mathematical basis of combination of the receptance method and flutter margin. In Eq. (29), the number of equations is $5k$, and the unknown variables include $k_1, k_2, \mathbf{g}, \mathbf{f}$, and $\beta_{1j} \pm \mathrm{i}\omega_{1j}, \beta_{2j} \pm \mathrm{i}\omega_{2j}, j = 1, \cdots, k$, so the number of unknowns is $4k + 2m + 2$. If the set of equations have a unique solution, $5k = 4k + 2m + 2$ should be satisfied, that is the number of design points k should be $2m + 2$. For the model shown in Fig. 1, k should not be less than 6.

In fact, Eq. (29a) is hard to be satisfied strictly. It is more rational that the problem of solving Eq. (29) is transformed into a problem of optimization. So active flutter suppression can be described as follows:

Given the measured open-loop receptances $\mathbf{h}_j(s)$ at airspeed V_j, $j = 1, \cdots, k$ and the desired flutter boundary V_f, search for the control gains $\mathbf{g}^\mathrm{T} = [g_1 \quad g_2]$, $\mathbf{f}^\mathrm{T} = [f_1 \quad f_2]$, and the coefficients k_1, k_2, such that

$$\begin{aligned} \text{minimize} \quad & \sum_{j=1}^{k} \left[F(\beta_{1j}, \omega_{1j}, \beta_{2j}, \omega_{2j}) - k_1(V_j^2 - V_\mathrm{f}^2) - k_2(V_j^2 - V_\mathrm{f}^2)^2\right]^2 \\ \text{subject to} \quad & 1 + \left(\mathbf{g} + (\beta_{1j} \pm \mathrm{i}\omega_{1j})\mathbf{f}\right)^\mathrm{T} \mathbf{h}_j(\beta_{1j} \pm \mathrm{i}\omega_{1j}) = 0, \quad j = 1, \cdots, k \\ & 1 + \left(\mathbf{g} + (\beta_{2j} \pm \mathrm{i}\omega_{2j})\mathbf{f}\right)^\mathrm{T} \mathbf{h}_j(\beta_{2j} \pm \mathrm{i}\omega_{2j}) = 0, \quad j = 1, \cdots, k \end{aligned} \tag{30}$$

In above optimization problem, the limit to the number of design points k is not necessary. Sometimes redundant design points may cause the solution search to fail. For the cases studied in this paper, the number of design points was chosen between 4 to 6.

D. Strategy of Optimization

Combining the receptance method and flutter margin, the active flutter suppression problem has been transformed to the optimization of a multi-modal function. As Eq. (30) is highly nonlinear, the gradient optimization methods (such as the gradient descent method or the conjugate gradient method) could not work well. So a non-gradient optimization method (genetic algorithm[20]) is applied to find the optimal solution of Eq. (30). The flowchart of the solution searching is shown as Fig. 2.

1. Initialize the group. The genes of individuals denote the possible values of g_1, g_2, f_1, f_2, and k_1, k_2.

2. For each design point, solve roots of Eq.(26) to obtain the poles $\beta_{1j} \pm \mathrm{i}\omega_{1j}, \beta_{2j} \pm \mathrm{i}\omega_{2j}$. The receptance matrix obtained by curve fitting is expressed as

$$\mathbf{h}(s) = \frac{1}{D(s)} \begin{bmatrix} N_1(s) \\ N_2(s) \end{bmatrix} \tag{31}$$

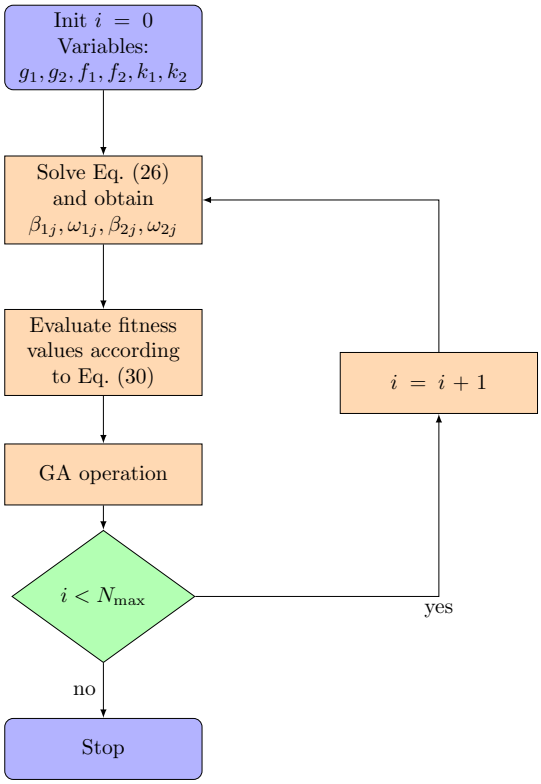

Figure 2. The Flowchart of Seeking Control Gains

where $N_1(s)$, $N_2(s)$ and $D(s)$ are algebraic polynomials. So solving Eq. (26) is equivalent to solving the roots of the polynomial equation

$$D(s) + (g_1 + sf_1)N_1(s) + (g_2 + sf_2)N_2(s) = 0 \tag{32}$$

Standard numerical algorithms (such as Newton's method or eigenvalue algorithm) can be used for solving roots. Usually the number of roots is greater than 2, so the most important thing is to find the right poles which represent the flutter modes, and therefore prior knowledge about the flutter characteristic of the system can be useful.

3. Evaluate the fitness values of individuals in the group. The fitness function is defined as the objective function.

4. Genetic algorithm operation on individuals, including sorting, selecting, re-combine, mutation, and re-insert.

5. If iteration number $< N_{\max}$, go to Step 2 and iterate.

IV. Test Cases

A. Dynamics of Open-Loop

The basic parameters of the uniform cantilever wing are listed in Table 1. In this work, 4 bending modes and 4 torsional modes are considered in theoretical flutter analysis and validation of flutter suppression. For the sake of simplicity, the dynamics of the actuator is not considered in this test case (its transfer function $r(s)$ is assumed to be 1).

Based on the values of the parameters, the theoretical flutter analysis is conducted by two methods. One is the classical p-k method,[21] which gives the damping ratios and frequencies of all the modes at the speed points (V-g and V-f plots). The other is the flutter margin method. Four speed points were selected for

Table 1. Parameters of the Uniform Cantilever Wing

Parameter	Value	Parameter	Value
c	2.0 m	C_l^θ	2π
l	7.5 m	C_l^β	2.478
m	200 kg/m^2	$C_m^{\dot\theta}$	-1.2
x_f	0.48 c	C_m^β	-0.540
EI	2.0×10^7 Nm^2	ρ	1.225 kg/m^3
GJ	2.0×10^6 Nm^2	$r(s)$	1

flutter evaluation, that is $V = 60, 65, 70, 75$ m/s. At each speed point, the poles of the flutter modes (in this case, they are 1st and 2nd modes) were calculated, and the flutter margin evaluated. By using curve fitting, the flutter boundary was predicted. The analysis results obtained by the two methods are shown in Fig. 3. The p-k method gives the flutter speed of the open-loop system $V_\mathrm{f} = 80.8$ m/s and flutter frequency $\omega_\mathrm{f} = 3.43$ Hz. The flutter margin method predicts $V_\mathrm{f} = 80.9$ m/s. The results of the two methods are in good agreement.

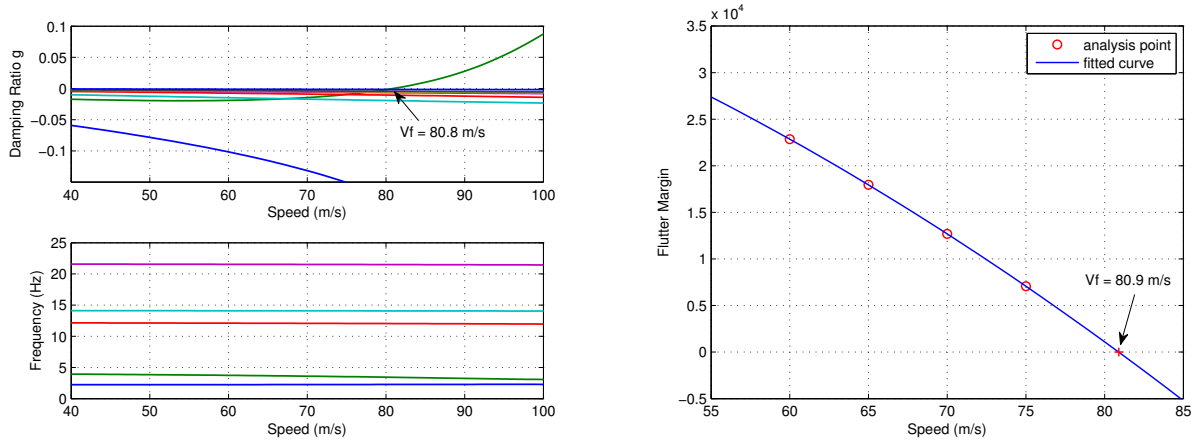

(a) resluts of the p-k method

(b) results of the flutter margin method

Figure 3. Theoretical Flutter Analysis Results of the Open-Loop System

For control law design of the active flutter suppression system, the speed points of $V = 60, 65, 70, 75$ m/s were selected as the design points. The receptances of the open-loop were calculated at the sampled frequencies based on the theoretical system model, as shown in Fig. 4. By using rational fraction polynomials fit in the interested frequency range (0–10 Hz), the receptances can be expressed as the following 6-order rational fraction polynomials.

$$h_{1,2}(s) = \frac{a_5 s^5 + a_4 s^4 + a_3 s^3 + a_2 s^2 + a_1 s + a_0}{b_6 s^6 + b_5 s^5 + b_4 s^4 + b_3 s^3 + b_2 s^2 + b_1 s + 1}$$

B. Active Flutter Suppression

In this section, the desired flutter speed of the closed-loop is set to $V_\mathrm{f}^* = 90$. In solution searching of genetic algorithm, the number of individuals is 100, and the maximum number of generations is 80. Fig. 5 shows a obvious descent of the value of objective function in the iteration process. A set of obtained optimal solutions is listed in Table 2.

To verify the effect of flutter suppression, flutter analysis of the closed-loop was conducted by the p-k method and the flutter margin method, and the analysis results are shown in Fig. 6. The closed-loop flutter speed based on the theoretical system model is $V_\mathrm{f} = 90.2$ m/s, while the flutter speed predicted by the flutter

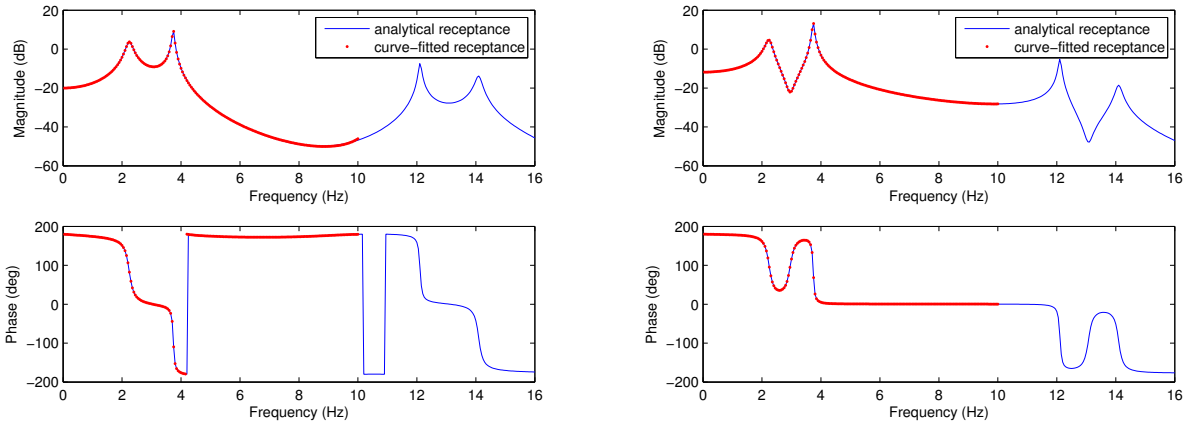

(a) $h_1(s)$ (b) $h_2(s)$

Figure 4. Receptances of the Open-Loop System at the Design Ponit of $V = 60$ m/s

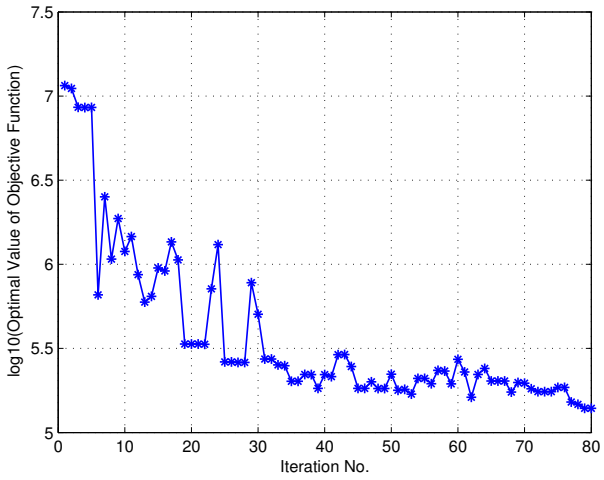

Figure 5. Objective Function Values in the Iteration Process

Table 2. Results of Optimization for $V_{\mathrm{f}}^* = 90$ m/s

Design Variable	g_1	g_2	f_1	f_2	k_1	k_2
Value	0.1012	0.4640	0.0143	-0.0047	-8.7826	-0.00061

margin is $V_{\mathrm{f}} = 91.1$ m/s. There is a little difference between the flutter results of the two methods, which is due to errors in optimization and flutter prediction.

To evaluate the practicability of the control gains, a MATLAB/Simulink model (Fig. 7) is established and aeroelastic response analysis in time domain is implemented by simulation. At the airspeed of $V = 85$ m/s, a $1-$cosine discrete gust ($\max(w_g)$=10 m/s, and length of wave $L_{\mathrm{g}} = 50$ m) is considered as a disturbance. The responses of the receiver points on wing-tip and the deflection of control surface are shown in Fig. 8. The results show that the active controller can prevent flutter effectively, and the deflection of control surface maintains a reasonable range.

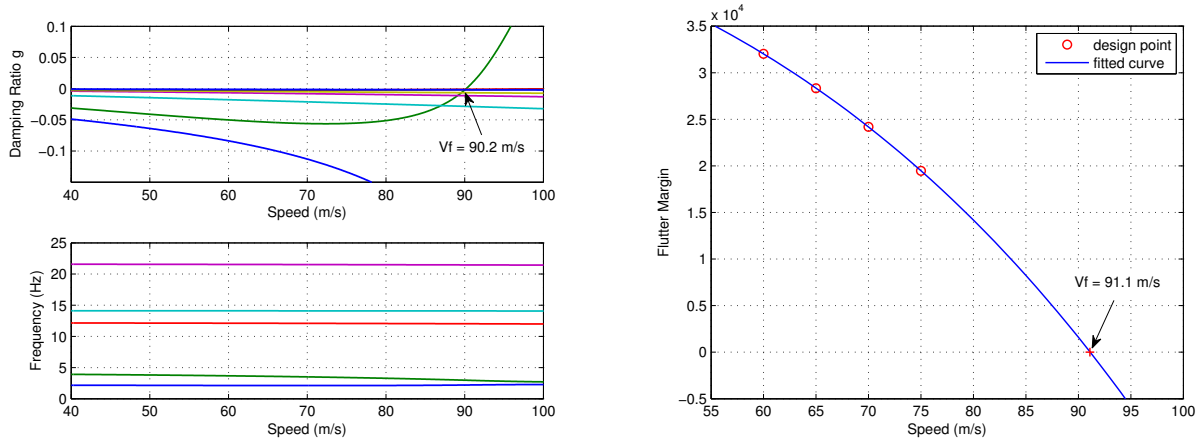

(a) resluts of the p-k method (b) results of the flutter margin method

Figure 6. Flutter Analysis Results of the Closed-Loop System ($V_f^* = 90$ m/s)

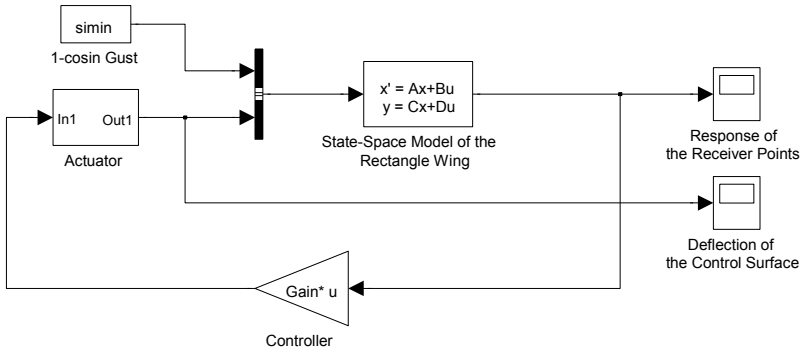

Figure 7. The MATLAB/Simulink model of the Closed-Loop System

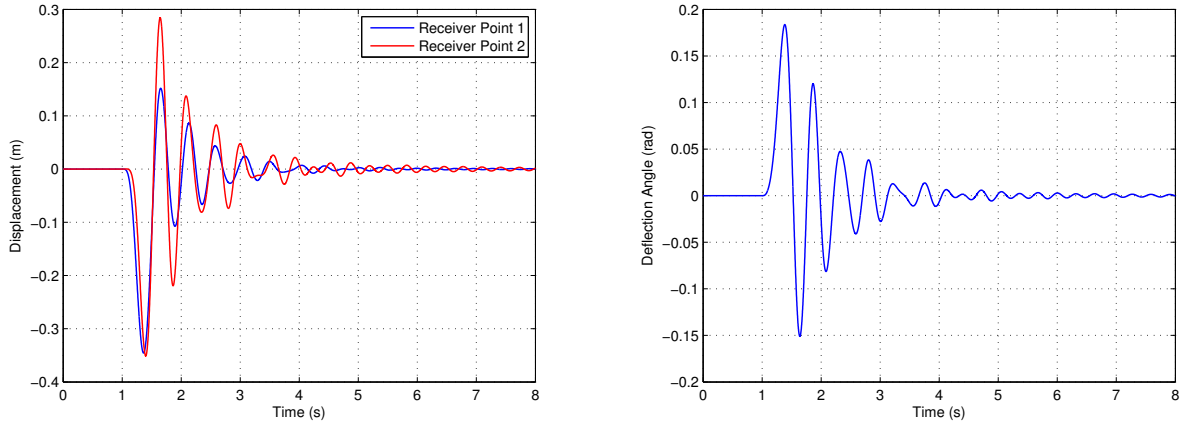

(a) displacements of the receiver points (b) deflection of the control surface

Figure 8. Time Responses of the Closed-Loop System Under a Discrete Gust ($V = 85$ m/s)

C. Further Investigation

1. Randomness of Solutions

Because the optimization method is a random strategy, and the solutions to the problem are not unique, so the optimal results of different runs of calculation are not the same. Table 3 and Fig. 9 show the optimal

results of 4 runs and their flutter suppression effects. There are big differences between control gains in different runs, while all the closed-loop flutter speeds are close to the desired target $V_f^* = 90$ m/s. There are also some differences between the flutter speeds evaluated by the flutter margin method and the p-k method.

Table 3. Solutions of Control Gains Searching (4 Design Points, $V_f^* = 90$ m/s)

Run No.	g_1	g_2	f_1	f_2	V_{f1} (m/s)	V_{f2} (m/s)
1	0.1012	0.4640	0.0143	-0.0047	91.1	90.2
2	-0.1053	0.4199	0.0095	-0.0045	91.3	90.9
3	0.2095	0.2369	0.0135	-0.0025	89.1	88.3
4	-0.0970	0.3148	0.0110	-0.0033	91.2	90.3

Note: V_{f1} is the flutter speed predicted by flutter margins,
V_{f2} is the flutter speed based on theoretical model.

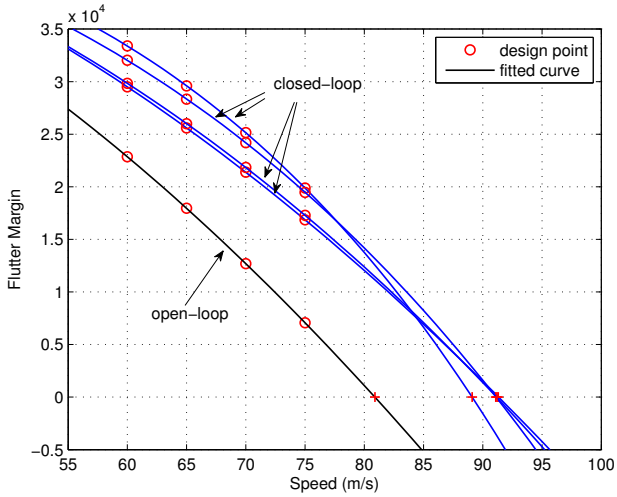

Figure 9. Flutter Margins and Prediction of the Closed-Loop System (4 Design Points, $V_f^* = 90$ m/s)

The time responses of the closed-loop system by using control gains of different runs are also compared, as shown in Fig. 10. The results show the required deflection of the control surface are different, though the active controllers of different runs achieve the same effect of flutter suppression.

2. Number of Design Points

To study the influence of the number of design points, the control design in cases of 5 and 6 design points is conducted. For the case of 5 design points, the airspeed is $V = 60, 65, 70, 75, 79$ m/s. For the case of 6 design points, the airspeed is $V = 55, 60, 65, 70, 75, 79$ m/s. Table 4 and Table 5 list the optimal results of 4 runs and flutter speeds of the closed-loop. It seems that the accuracy of the achieved flutter speed becomes better in cases of more design points.

Fig. 11 shows the flutter margins and predictions of the closed-loop system in the cases of 5 and 6 design points. The results indicate that there are multiple solutions which satisfy Eq. (29). It is difficult to find the solutions by using the traditional gradient methods, but the random search method can work well.

3. Influence of Desired Flutter Speed

To study the influence of the desired flutter speed, control gains design in the cases of the desired flutter speed $V_f^* = 85, 90, 95$ m/s is implemented, and the optimization results are shown in Table 6. Fig. 12 shows the flutter margin curves of the closed-loop for different desired flutter speeds. In the speed range of 85–100 m/s, the effect of flutter suppression can be achieved accurately by using the presented method.

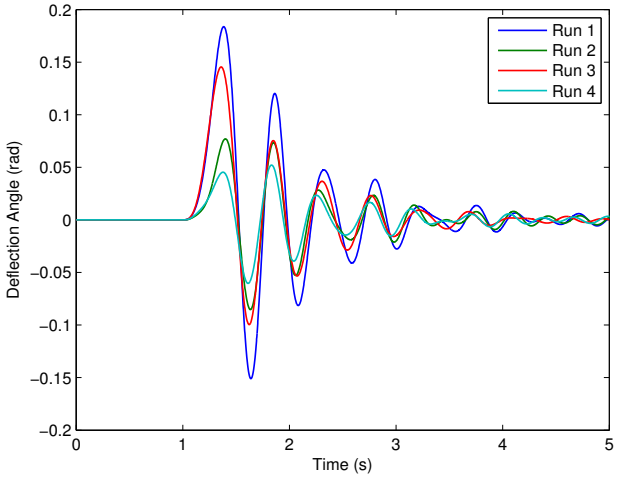

Figure 10. Comparison of Response of Control Surface between Different Runs

Table 4. Solution of Control Gains Searching (5 Design Points, $V_f^* = 90$ m/s)

Run No.	g_1	g_2	f_1	f_2	V_{f1} (m/s)	V_{f2} (m/s)
1	-0.2053	0.2617	0.0107	-0.0017	89.8	89.3
2	0.1892	0.1726	0.0081	-0.0040	89.7	89.7
3	-0.3885	0.4437	0.0141	-0.0005	91.0	89.5
4	0.1024	0.3901	0.0009	-0.0066	90.5	90.7

Note: V_{f1} is the flutter speed predicted by flutter margins,
V_{f2} is the flutter speed based on theoretical model.

Table 5. Solution of Control Gains Searching (6 Design Points, $V_f^* = 90$ m/s)

Run No.	g_1	g_2	f_1	f_2	V_{f1} (m/s)	V_{f2} (m/s)
1	-0.2053	0.2617	0.0107	-0.0017	90.0	89.8
2	0.1892	0.1726	0.0081	-0.0040	89.9	89.9
3	-0.3885	0.4437	0.0141	-0.0005	89.7	89.9
4	0.1024	0.3901	0.0009	-0.0066	89.9	90.1

Note: V_{f1} is the flutter speed predicted by flutter margins,
V_{f2} is the flutter speed based on theoretical model.

It should be noted that the control law effectiveness in case of $V_f^* = 95$ m/s a slightly larger error than others. In fact, control design in the case of $V_f^* = 100$ m/s is also conducted, but the results of different runs are scattered, and the flutter speed of the closed-loop can not focus on the target. Numerical studies indicate that the extension of flutter boundary is limited. If the desired flutter is highly greater than the maximum speed of design points, the coupling mechanism of flutter become difficult to predict, and the present method may not work well.

4. Influence of Accuracy of Receptances

In above numerical studies, the receptances were obtained from the theoretical system model, and measure errors are not considered. To simulate realistic condition, a virtual experiment based on MATLAB/Simulink simulation is implemented. The simulation model is shown in Fig. 13. In the virtual experiment, a burst random signal was chosen as a input to excite the open-loop system, and the responses of the receiver points

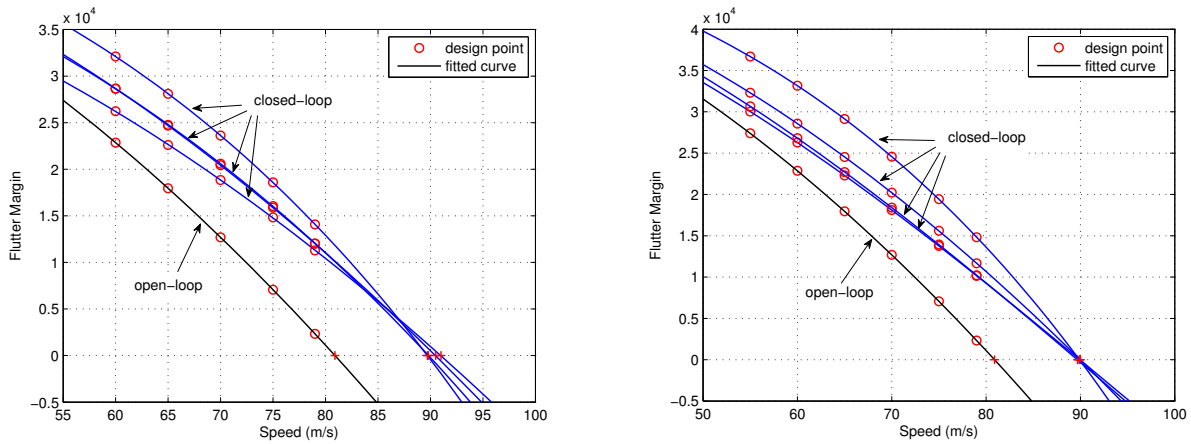

(a) 5 design points

(b) 6 design points

Figure 11. Flutter Margins and Predictions of the Closed-Loop System (More Design Points, $V_f^* = 90$ m/s)

Table 6. Solutions of Control Design for Different Desired Flutter Speeds

Target V_f^*	g_1	g_2	f_1	f_2	V_{f1} (m/s)	V_{f2} (m/s)
85	-0.0775	0.4236	0.0033	-0.0008	85.3	85.4
90	-0.2053	0.2617	0.0107	-0.0017	89.8	89.3
95	-0.0003	0.4109	0.0130	-0.0089	94.1	93.8

Note: V_{f1} is the flutter speed predicted by flutter margins,
V_{f2} is the flutter speed based on theoretical model.

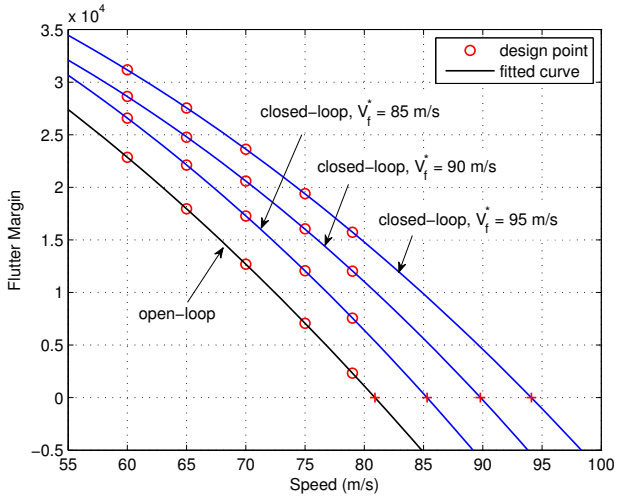

Figure 12. Flutter Margin Curves of the Closed-Loop in cases of $V_f^* = 85, 90, 95$ m/s

are recorded as outputs. After spectrum analysis and averaging, the simulated experiment receptances and their curve fitting can be obtained, which are shown in Fig. 14.

The solutions of control gains searching based on the simulated experiment receptances are listed in Table 7. It shows that the closed-loop flutter speed predicted by the flutter margins is still close to the desired target, but there is a greater difference between the theoretical flutter speed and the desired target. In fact, the errors of receptances can be transmitted to the poles of closed-loop, flutter margin of design points, and the predicted flutter speed. To obtain the satisfied flutter suppression, the errors of receptances

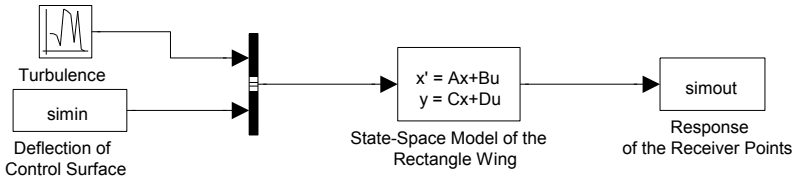

Figure 13. The Simulation Model for the Virtual Experiment of the Open-Loop

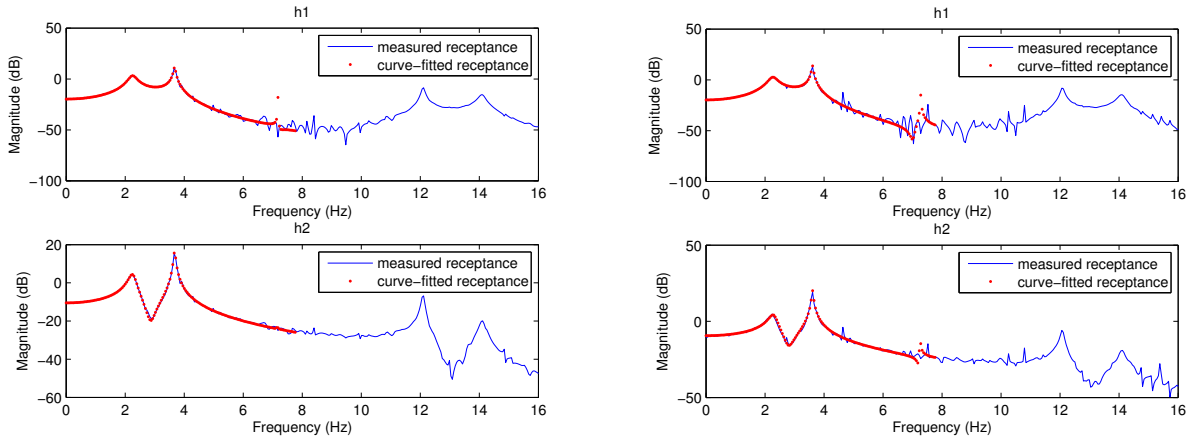

(a) $V = 65$ m/s (b) $V = 70$ m/s

Figure 14. The Simulated Experiment Receptances and Curve Fitting

should be reduced as much as possible.

Table 7. Solution of Control Gains Searching Based on the Simulated Experiment Receptances

Run No.	g_1	g_2	f_1	f_2	V_{f1} (m/s)	V_{f2} (m/s)
1	-0.1868	0.4110	0.0084	-0.0062	90.7	93.0
2	-0.2099	-0.0216	0.0114	-0.0019	91.2	91.2
3	-0.0242	-0.0518	0.0105	-0.0019	89.5	89.5
4	-0.1190	0.2945	0.0046	-0.0066	90.3	94.0

Note: V_{f1} is the flutter speed predicted by flutter margins,
V_{f2} is the flutter speed based on theoretical model.

V. Application

To validate the practicability of combination of the receptance method and flutter margin, active flutter suppression for a realistic wing is implemented. The finite element model of a regional jet wing is composed of beams and lumped masses, as shown in Fig. 15(a). Unsteady aerodynamics calculation is implemented by the doublet lattice method (DLM), and the aerodynamic model is shown in Fig. 15(b). The frequencies of the first 4 structural modes are 2.04, 6.38, 13.66, 13.90 Hz, and the corresponding mode shapes are shown in Fig. 16.

To acquire the prior knowledge of the flutter coupling mechanism, a numerical flutter analysis was conducted by the p-k method and the flutter margin method. The analysis results obtained by the two methods are shown in Fig. 17. The p-k method gives the flutter speed of the open-loop system $V_f = 266$ m/s and flutter frequency $\omega_f = 8.43$ Hz. In flutter margin analysis, the poles which represent 1st mode and 3rd mode are applied to evaluate flutter margin, and obtain $V_f = 260$ m/s. The results of the two methods are in good agreement and indicate 1st mode and 3rd mode are dominant flutter modes.

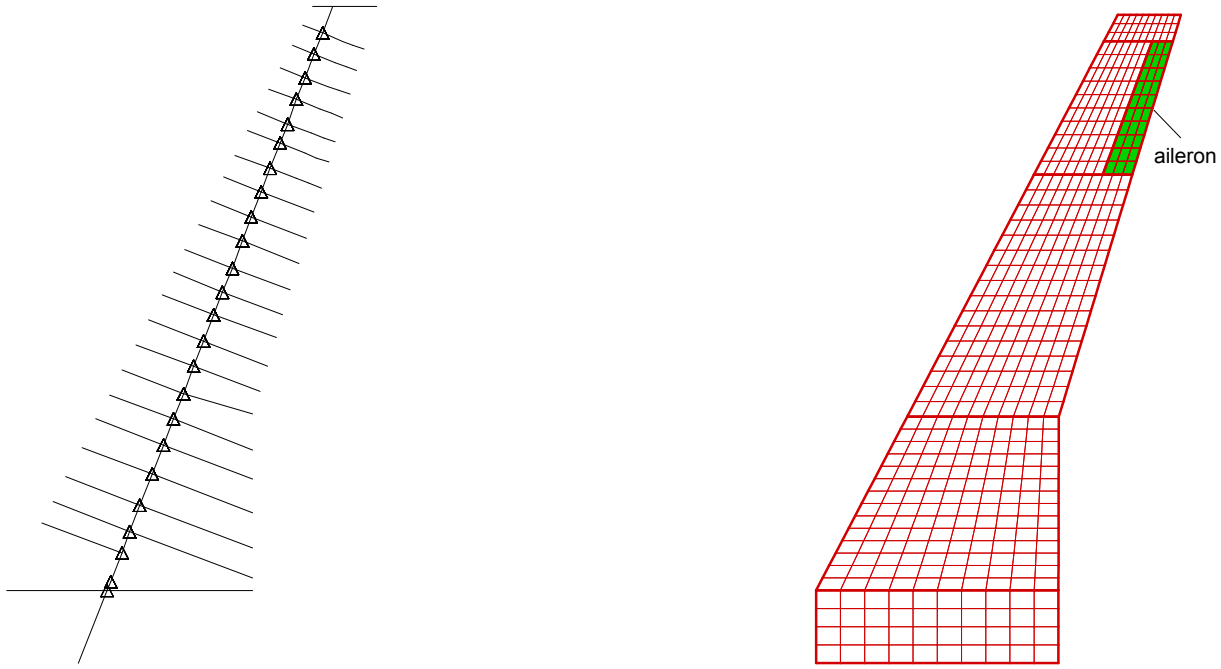

(a) Structural Model (b) Aerodynamic Model

Figure 15. Structural and Aerodynamic Models of a Regional Jet Wing

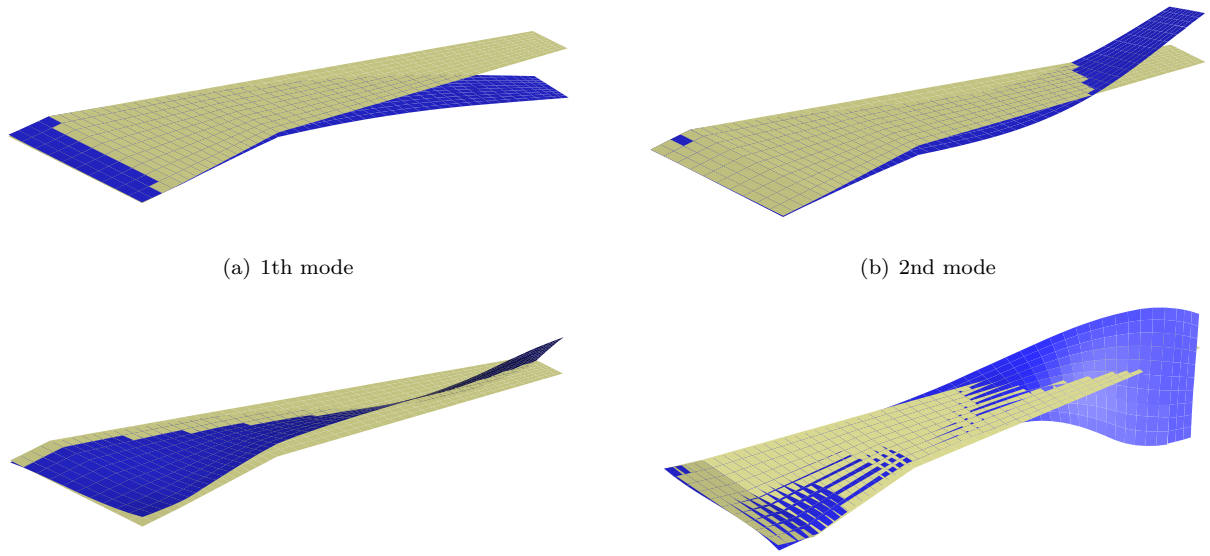

(a) 1th mode (b) 2nd mode

(c) 3rd mode (d) 4th mode

Figure 16. The First 4 Mode shapes of the Wing

For active flutter suppression, the trailing-edge on the wing-tip is chosen as the receiver point, and the aileron is set as the control surface. The dynamics of the actuator driving the aileron is considered, and its model is specified by a transfer function having the form

$$G_{\mathrm{a}}(s) = \frac{a}{s+a} \cdot \frac{\omega^2}{s^2 + 2\xi\omega s + \omega^2} \tag{33}$$

Conducting the rational function approximation of unsteady aerodynamics coefficients, a state-space model of open-loop aeroelastic system[22] is established. This theoretical model is used to obtain receptances

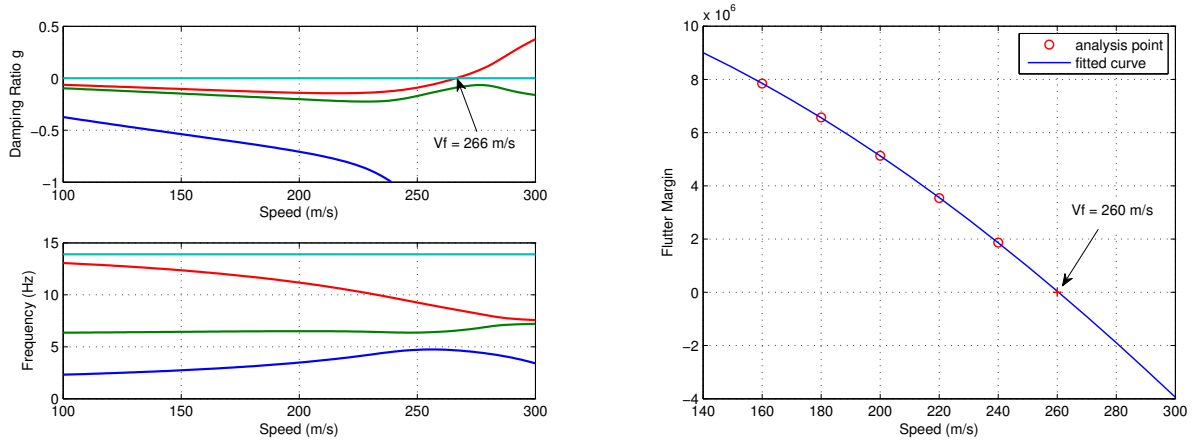

(a) resluts of the p-k method

(b) results of the flutter margin method

Figure 17. Theoretical Flutter Analysis Results of the Jet Wing

and validate flutter suppression. In this case, $V = 160, 180, 200, 220$ m/s are selected as the design points, and the desired flutter speed is set to 280 m/s. A set of solution of control gains is listed in Table 8, and the flutter margin curves are shown in Fig. 18. Results show that the designed control gains achieve the desired target.

Table 8. Solutions of Control Design for Different Desired Flutter Speeds

Target V_f^*	g	f	V_{f1} (m/s)	V_{f2} (m/s)
280	0.4700	0.6670	288	278

Note: V_{f1} is the flutter speed predicted by flutter margins,
V_{f2} is the flutter speed based on theoretical model.

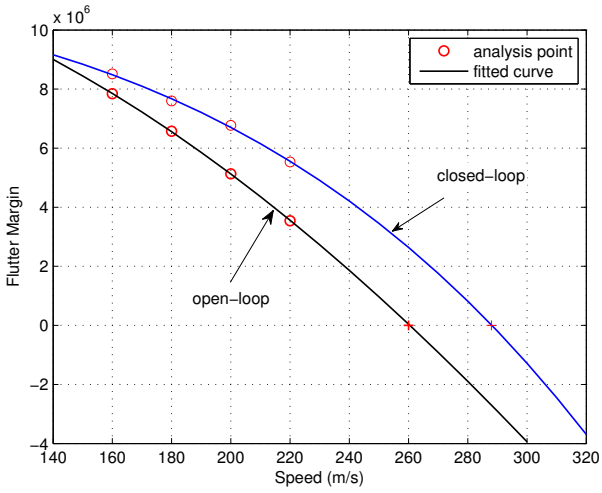

Figure 18. Flutter Margins of the Jet Wing (4 Design Points, $V_f^* = 280$ m/s)

VI. Conclusions

A novel approach of active flutter suppression, using a combination of receptance method and flutter margin technique is developed in this paper. The approach inherits the advantage of the receptance method

and overcome a weakness in its implementation. The feedback control gains are based upon measured receptances, without need to know the mass, damping, and stiffness matrices of the system. Moreover, applying the flutter margin technique, inappropriate pole-assignment is avoided. In this approach, the control gains design is transformed into a optimization problem, and the genetic algorithm was used to search the optimal solution. Given the measured open-loop receptances at the design points and the desired flutter boundary, the obtained control gains can effectively extend the flutter boundary to the target.

Design of output feedback control for a multi-degree-of-freedom uniform wing numerical model with a trailing-edge control surface is demonstrated, and application to a realistic jet wing is also introduced. Numerical results show that the presented approach can effectively extend the flutter boundary without the usual difficulties of pole-assignment. Further studies indicate that proper selection of design points can improve the effect of flutter suppression, while the errors on the receptances can have a detrimental influence on the results.

Acknowledgments

This work was supported by the National Natural Science Foundation of China (grant No. 11372023) and the Royal Academy of Engineering.

References

[1]Wright, J. R. and Cooper, J. E., *Introduction to Aircraft Aeroelasticity and Loads*, John Wiley & Sons, Ltd Press, 2007.

[2]Sandford, M. C., Abel, I., and Gray, D. L., "Development and Demonstration of a Flutter-Suppression System Using Active Controls," NASA TR R–450, 1975.

[3]Waszak, M. R. and Srinathkumar, S., "Flutter Suppression for the Active Flexible Wing: Control System Design and Experimental Validation," AIAA–92–2097–CP, 1992.

[4]Mukhopadhyay, V., "Flutter Suppression Control Law Design and Testing for the Active Flexible Wing," *Journal of Aircraft*, Vol. 32, No. 1, 1995, pp. 45–51.

[5]Waszak, M. R., "Robust Multivariable Flutter Suppression for Benchmark Active Control Technology Wind-Tunnel Model," *Journal of Guidance, Control and Dynamics*, Vol. 24, No. 1, 2001, pp. 147–153.

[6]Ku, K. S. and Hajela, P., "Neural-Network-Based Controller for Nonlinear Aeroelastic System," *AIAA Journal*, Vol. 36, No. 2, 1998, pp. 249–255.

[7]Ram, Y. M. and Mottershead, J. E., "Receptance Method in Active Vibration Control," *AIAA Journal*, Vol. 45, No. 3, 2007, pp. 562–567.

[8]Mottershead, J. E., Tehrani, M. G., James, S., and Ram, Y. M., "Active Vibration Suppression by Pole-Zero Placement Using Measured Receptances," *Journal of Sound and Vibration*, Vol. 311, No. 35, 2008, pp. 1391–1408.

[9]Mottershead, J. E. and Ram, Y. M., "Inverse eigenvalue problems in vibration absorption: Passive modification and active control," *Mechanical Systems and Signal Processing*, Vol. 20, No. 1, 2006, pp. 5–44.

[10]Singh, K. V., McDonough, L., Mottershead, J. E., and Cooper, J. E., "Active Aeroelastic Control Using the Receptance Method," *Proceedings of the ASME International Mechanical Engineering Congress and Exposition (IMECE-10)*, IMECE2010–38877, 2010, pp. 137–146.

[11]Mcdonough, L., *Receptance Based Control of Aeroelastic Systems for Flutter*, Ph.D. thesis, Miami University, 2012.

[12]Papatheou, E., Tantaroudas, N. D., Ronch, A. D., Cooper, J. E., and Mottershead, J. E., "Active control for flutter suppression: an experimental investigation," *International Forum on Aeroelasticity and Structural Dynamics (IFASD)*, IFASD Paper 2013-8D, 2013.

[13]Singh, K. V., McDonough, L. A., Kolonay, R., and Cooper, J. E., "Receptance-Based Active Aeroelastic Control Using Multiple Control Surfaces," *Journal of Aircraft*, Vol. 51, No. 1, 2014, pp. 335–342.

[14]Tehrani, M. G., Wilmshurst, L., and Elliott, S. J., "Receptance method for active vibration control of a nonlinear system," *Journal of Sound and Vibration*, Vol. 332, No. 19, 2013, pp. 4440–4449.

[15]Zhen, C., Li, D., and Xiang, J., "A Modified Receptance Method for Active Control of a Nonlinear Aeroelastic System," *56th AIAA/ASCE/AHS/ASC Structures, Structural Dynamics, and Materials Conference*, Kissimmee, Florida, January, 2015.

[16]Golub, G. H. and van Loan, C. F., *Matrix Computations*, Johns Hopkins University Press, 1983.

[17]Richardson, M. H. and Formenti, D. L., "Parameter Estimation from Frequency Response Measurements Using Rational Fraction Polynomials," *1st IMAC Conference*, Orlando, Florida, November, 1982.

[18]Zimmerman, N. H. and Weissenburge, J. T., "Prediction of Flutter Onset Speed Based on Flight Testing at Subcritical Speeds," *Journal of Aircraft*, Vol. 1, No. 4, 1964, pp. 190–202.

[19]Dimitriadis, G. and Cooper, J. E., "Flutter Prediction from Flight Flutter Test Data," *Journal of Aircraft*, Vol. 38, No. 2, 2001, pp. 355–367.

[20]Chipperfield, A. J., Fleming, P. J., and Fonseca, C. M., "Genetic Algorithm Tools for Control Systems Engineering," *Proc. Adaptive Computing in Engineering Design and Control*, Plymouth Engineering Design Centre, UK, September 21-22, 1994.

[21]Rodden, W. P. and Johnson, E. H., *MSC/NASTRAN Version 68 Aeroelastic Analysis User's Guide*, MacNeal-Schwendler Corp., 1994.

[22] *ZAERO Version 8.2 Theoretical Manual*, ZONA Technology, Inc., 2008.